Article

Daylight-Active Cellulose Nanocrystals Containing Anthraquinone Structures

Yiwen Zhu[1], Audrey Sulkanen[2], Gang-Yu Liu[2], and Gang Sun[1,*]

[1] Department of Biological and Agricultural Engineering, University of California, Davis, One Shields Avenue, Davis, CA 95616, USA

[2] Department of Chemistry, University of California, Davis, One Shields Avenue, Davis, CA 95616, USA

* Correspondence: Gang Sun at: 235 Everson, University of California, Davis, One Shields Avenue, Davis, CA 95616; Email address: gysun@ucdavis.edu

Received: date; Accepted: date; Published: date

Abstract: Antimicrobial and anti-viral materials have attracted significant interest in recent years due to increasing occurrences of nosocomial infections and pathogenic microbial contamination. One method to address this is the combination of photoactive compounds that can produce reactive oxygen species (ROS), such as hydrogen peroxide and hydroxyl radicals to disinfect microbes, with carrier materials that meet the application requirements. Using anthraquinone (AQ) and cellulose nanocrystals (CNCs) as the photoactive and carrier components respectively, this work demonstrates the first covalent incorporation of AQ onto CNCs. The morphology and the photoactive properties were investigated, revealing the structural integrity of the CNCs, and high degree of photoactivity of AQ-CNC materials upon UVA exposure. The AQ-CNCs also exhibited an unexpected persistent generation of ROS under darkness, which adds advantages for antimicrobial applications.

Keywords: Cellulose Nanocrystal; Anthraquinone; Reactive Oxygen Species; FTIR; Atomic Force Microscopy

1. Introduction

Antimicrobial and anti-viral materials have been a growing field of interest for researchers due to increasing nosocomial infections and pathogenic microbial contaminations. Considerable effort has been devoted to developing surfaces with biocidal functions and self-disinfecting properties[1-3], as such modified surfaces could incorporated in sterile garments and fabrics, thereby reducing the possibility of microbial and/or viral contamination.

In this pursuit, the functionalization of materials with light reactive groups could be used to reduce microbial contamination and viral infection [4]. Species that can absorb long wavelength ultraviolet light (UVA) or daylight and become excited to produce reactive oxygen species (ROS) including hydrogen peroxide, hydroxyl radicals and even singlet oxygen [5,6] are ideal candidates as functional groups. The ROS would provide antibacterial and self-disinfecting properties for the modified materials, as well as being environmentally friendly since they only require light exposure and oxygen to function [7-10].

In selecting a light reactive species, anthraquinone derivatives are promising candidates, as they are known for being light-active under daylight or UVA exposure. The addition of these anthraquinone derivatives to solutions and materials has been shown to produce significant amounts of ROS, resulting in light-induced antibacterial functions [7,8]. While successful in ROS generation, the possible leaching of these colorants from the materials needs to be addressed [8]. One means of addressing this issue is the covalent linkage of the light active agents to the substrate.

Chemical incorporation of light-active agents onto polymers has been explored as a successful method to prevent leaching. Surface modification and functionalization of cellulose with anthraquinone dyes has demonstrated durable light-induced antimicrobial properties on cotton fibers [11] while preventing the leaching of the agents from the fabrics. Applying this chemical modification to nanomaterials provides a means to expand the utility of these hybrid materials while preventing leaching related complications.

In terms of potential carrier materials, cellulose nanocrystals (CNCs) stand out as prospective candidates, as they are produced from agricultural wastes and are considered renewable and sustainable materials [12,13]. Cellulose nanomaterials modified with photoactive group also have promising biomedical applications. Cellulose nanocrystals (CNCs) are normally produced by acid hydrolysis of cellulose to result in nanometer sized materials with unique structural features. These CNCs are functionalized with covalent sulfate ester groups on their surfaces due to the hydrolysis with sulfuric acid [14]. These sulfate groups make the CNCs easy to disperse in water but also hinder the incorporation of other functional groups [15,16]. Removal of the sulfate ester groups can be achieved following previously described procedures [17,18], and these partially desulfated CNCs can react with a light-active species, such as anthraquinone, to create non-leaching functionalized CNCs.

This work reports the first success in directly and covalently linking an anthraquinone derivative onto the surfaces of CNCs. Utilizing a variety of analytical techniques, the chemical and morphological structures and characteristics of AQ-CNCs were investigated, and the results of their photo active properties represent a significant step forward in the development of anti-microbial hybrid materials using CNCs.

2. Materials and Methods

2.1 Materials

Cellulose microcrystalline (Acros), sulfuric acid (96.2%, Fisher Scientific), sodium hydroxide (97%, Fisher Scientific), sodium chloride (99%, Fisher Scientific), anthraquinone-2-carboxylic acid (99%, Tokyo Chemical Industry CO.), N, N'-carbonyldiimidazole (CDI) (98%, Oakwood Chemical), N,N-dimethylformamide (DMF) (99.9%, Sigma-Aldrich), dimethyl sulfoxide (DMSO) (99.9%, Sigma-Aldrich), magnesium sulfate (97%, Sigma-Aldrich), potassium bromide (99%, Acros), Poly-L-lysine solution (0.1 w/v in H_2O, Sigma) and ethyl alcohol (95%, Sigma-Aldrich) were used as received without any further purification. Muscovite mica pieces were mechanically peeled to reveal fresh (0001) surfaces before use. AC240TS-R3 silicon cantilevers were purchased from Oxford Instruments Asylum Research Water (≥18.2 MΩ) was purified by a Milli-Q system (Q-GARD 2).

2.2 Preparation of cellulose nanocrystals (CNCs)

Cellulose nanocrystals (CNCs) were prepared by sulfuric acid (H_2SO_4) hydrolysis of microcrystalline cellulose following a procedure reported previously [19]. The prevalence of sulfate groups on the surface was determined by conductometric titrations. The conductivity of the mixture was recorded by an Accumet XL600 benchtop meter (Fisher Scientific) with a conductivity electrode, AccuTupH conductivity/Temp probe (Fisher Scientific), against 0.02 M sodium hydroxide (NaOH).

Removal of the sulfate ester groups was achieved as previously described with minor charges [17]. The CNC suspension with sulfate ester groups was hydrolyzed in concentrated NaOH for 5 hours. The desulfated CNCs were then purified by repeated homogenization using DI water. Drops of 0.1 M H_2SO_4 were added into the mixture to neutralize the pH. The prevalence of residual sulfate groups on the desulfated cellulose nanocrystals (DS-CNCs) was determined by conductometric titration. 25 mg of DS-CNCs were dispersed in 20 mL DI water and sonicated with an ultrasonic liquid processor S4000 (Misonix Inc) for 5 min under 20% amplitude in an ice bath. The sulfated and desulfated cellulose nanocrystals suspensions were conditioned with 1 mM sodium chloride (NaCl) and then titrated with 0.02 M NaOH under continuously stirring. After each addition of NaOH, conductivity was measured after 1 minute to ensure that the conductivity value was stabilized. The conductivity of the mixture was recorded by an Accumet XL600 benchtop meter.

2.3 Surface functionalization of CNCs with AQC

Synthesis of anthraquinone-2-carboxylic acid (AQC) modified CNCs was performed in two steps as shown in Figure 1(a). First, AQC was dispersed in 30 mL dried dimethylformamide (DMF). Then 0.4004 g-0.8008 g of N,N'-carbonyldiimidazole (CDI) was dissolved in 10 mL of the dried DMF, and the solution was dropped into the AQC solution at 80 °C for 30 min under N_2 atmosphere to make the reaction mixture. Then, a total of 0.1 g DS-CNCs were dispersed in 10 mL dried DMF. After sonication at 30% amplitude for 5 min, the dispersed CNC suspension was added into the reaction mixture, followed by stirring at 80 °C for the specified reaction time under N_2 atmosphere. The final products were isolated with centrifugation and rinsed thoroughly with DMF and ethyl alcohol, respectively. Anthraquinone-2-carboxylic acid modified cellulose nanocrystal powder (AQ-CNC) was obtained after air-drying under dark conditions.

2.4 Characterizations of AQ modified CNCs

Fourier transform infrared (FTIR) spectroscopy of cellulose nanocrystals before and after functionalization was performed with a Nicolet 6700 FTIR spectrometer (Thermo Electron Co.) by using potassium bromide (KBr) pellets with a wave number range of 4000-400 cm^{-1}, resolution of 4 cm^{-1}, and 64 accumulations. The samples were mixed with KBr powder (2 mg sample mixed with 200 mg KBr) to prepare pellets. The relative abundance of ester bonds on AQ-CNCs can be calculated based on an intensity ratio of ester bond (1725 cm^{-1}) versus that of C-H bond (2898 cm^{-1}) measured by FTIR spectroscopy [20].

The ratios (grafting yields) of grafted anthraquinone moieties on the desulfated cellulose nanocrystals were quantified by measuring the absorbance of its DMSO suspension (0.200 g/L) at 331 nm with a UV-vis spectrophotometer Evolution 600 (Thermo Scientific) based on a calibration curve of AQC with CNCs in DMSO solutions.

Products of the CNC functionalizations (CNC, DS-CNC and AQ-CNC) were characterized using an atomic force microscope (MFP-3D, Asylum Research Corp., Santa Barbara, CA). Silicon probes, AC 240-TS (Olympus America, Central Valley, PA) with a nominal spring constant of 1.7 N/m, were used for imaging. Silicon probes were used after a brief cleaning in ethanol and drying under nitrogen as needed. All samples were imaged in tapping mode under ambient conditions. Poly-L-lysine coated-mica (0001) surfaces were prepared first peeling mica to expose the mica (0001) surface, then placing freshly cleaved mica in the 0.1% w/v Poly-L-Lysine solution for 10 minutes, and finally rinsing with milliQ water [21]. CNC Samples for atomic force microscopy (AFM) imaging were prepared by dispersing the crystals in milliQ water using an ultrasonic liquid processor S4000 (Misonix Inc) for 2.5 minutes (5 seconds on and 5 seconds off), with 30% amplitude in an ice bath. Solutions of functionalized CNCs were prepared at 0.002% w/v. After dispersion of CNCs in each solution, a 40 µL solution were deposited onto Poly-L-Lysine coated mica (0001) surfaces and allowed to dry in a clean and light-shielded container for at least 12 hours.

2.5 Detection of Hydroxyl Radicals

The production of hydroxyl radicals by AQ-CNCs was evaluated in DI water under UVA exposure and without UVA exposure conditions. The yields of hydroxyl radicals for the varied synthesis conditions were quantified indirectly by measuring photo-bleaching rates of a selective radical quencher, N, N-Dimethyl-4-nitrosoaniline (p-NDA). The bleaching rate of p-NDA in each sample was determined by monitoring the absorption of the mixture at the wavelength of λ_{max} (440 nm) with a UV-vis spectrophotometer as a function of illumination time. The UVA exposures of the mixtures were conducted in a Spectrolinker XL-1000, a UV cross-linker (Spectroline), with five 8 W UVA lamps (365 nm wavelength). The distance between the light source and samples was 12 cm. The light intensity in the cross-linker was 3 mW/cm^2.

2.6 Detection of Hydrogen Peroxide

Hydrogen peroxide generated by AQ-CNCs in the aqueous system under UVA (365 nm) irradiation was also quantified by an iodometric method. 10 mL 0.2 g/L AQ-CNC suspension samples prepared in a tube were irradiated under UVA light (365 nm wavelength) in the UV cross-linker with a light intensity of 3 mW/cm^2. For every designated testing duration, 0.1 mL of the sample was taken from the tube and diluted to 1 mL with DI water. The diluted sample was mixed

with 1 mL of Reagent A (contained 66 g/L potassium iodide (KI), 2 g/L sodium hydroxide (NaOH), and 0.2 g/L ammonium molybdate tetrahydrate ($(NH_4)_6Mo_7O_{24} \bullet 4H_2O$)) and 1 mL Reagent B (20 g/L potassium hydrogen phthalate (KHP)). The hydrogen peroxide reacted with iodide ions to give triiodide ions, which appeared as a dark brown color. The absorbance of the sample was measured spectrophotometrically at 351 nm with a UV-vis spectrophotometer (Evolution 600, Thermo Scientific), and the amount of H_2O_2 was calculated according to a standard calibration curve.

3. Results

3.1 Preparation and Characterization of AQ-CNCs

In theory, cellulose nanocrystals (CNCs) should possess sufficient numbers of hydroxyl groups for the intended incorporation of anthraquinone. However, sulfate groups on surfaces of CNCs introduced during the sulfuric acid catalyzed hydrolysis can potentially block the esterification reaction and reduce the yields of the reaction. Thus, a desulfation process by means of alkaline hydrolysis was applied to reduce or remove the sulfate groups on CNCs. Conductometric titrations were performed to compare the prevalence of sulfate groups on CNCs before and after the desulfation process. The titration curves are shown in Figure 1(b).

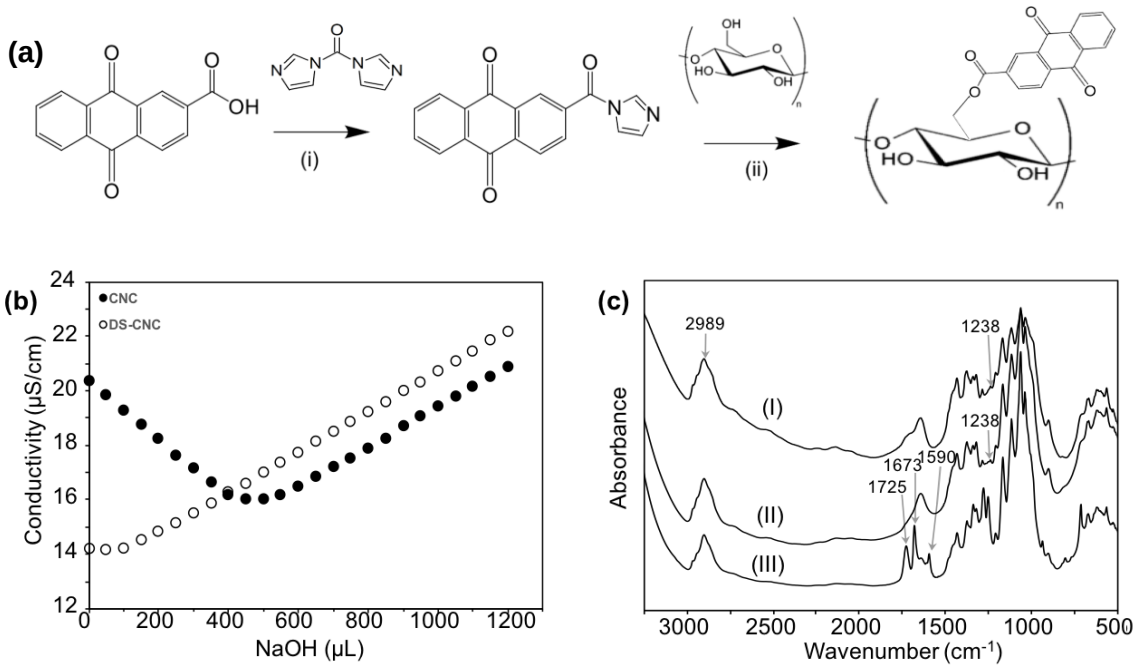

Figure 1. Preparation and characterization of desulfated CNC (DS-CNC) and AQ-CNC. (a) Synthesis of AQ-CNC (i) DMF, 80 ˚C, 0.5 hours; (ii) DMF, 80 ˚C, 2, 8, 12, and 24 hours respectively; (b) Conductometric titration curves of CNC samples; (c) FTIR of (I) CNC, (II) DS-CNC, (III) AQ-CNC.

NaCl was added into the suspension of CNCs as an electrolyte and contributes to the initial conductivity of the solutions. The counter ions of the sulfate groups, protons, contribute to the initial conductivity of the CNC samples and become reduced with the addition of sodium hydroxide initially. When sodium cations substituted all the protons, the conductivity started to increase due to further addition of sodium hydroxide. A subtle decrease and then immediate increase in conductivity represent the reduced sulfate contents on the DS-CNCs, confirming the significant reduction of sulfate groups on the DS-CNCs. The surface charge density σ, in mequiv/g, can be used as an indirect indication of the prevalence of sulfate groups, calculated from the titration results as

$$\sigma = \frac{c_{NaOH} \times V_{NaOH}}{c_{CNC} \times \alpha_{CNC}} \qquad (1)$$

where c_{NaOH} is the concentration of the titrant, V_{NaOH} is the titrant volume at the equivalence point, c_{CNC} is the concentration of the CNC suspension, and α_{CNC} is the amount of CNC

suspension titrated [18]. The surface charge density decreased from 0.36 mequiv/g to 0.04 mequiv/g after the desulfation process, indicating a significant reduction in the prevalence of sulfate groups. The lower absorbance intensity of S=O bonds at 1238 cm^{-1} on the DS-CNCs is shown in FTIR spectra in Figure 1(c(II)), also confirms the decrease of sulfate groups after the desulfation process [22].

The DS-CNCs were reacted with anthraquinone-2-carboxylic acid (AQC) to produce AQ grafted CNCs (AQ-CNCs) following an esterification reaction catalyzed by N,N′-carbonyldiimidazole (CDI), shown in Figure 1(a). The resulting AQ-CNCs were characterized by FTIR, and structural features of the ester and anthraquinone groups can be found on the spectra (III) in Figure 1(c). The peak at 1590 cm^{-1} is due to aromatic C=C stretching from the anthraquinone-2-carboxylic acid molecule and the peak of 1673 cm^{-1} is the carbonyl stretching peak on the anthraquinone group [11]. Another new peak at 1725 cm^{-1} is attributed to the ester group formed between DS-CNCs and AQC [11]. The band at 2898 cm^{-1} is the representative C-H bond in cellulose, which is not affected by the reaction.

All materials were subject to high-resolution AFM imaging to visualize fiber packing, and morphology and structures. AFM was selected as the technology choice due to its intrinsic advantages: (a) true 3D information; (b) label-free, and preserving materials native environments, in this case, ambient. AFM topographs are shown in Figure 2(a)-2(c), and examples of the individual CNCs are indicated in the images by oval enclosures. The AFM topographic images reveal that the individual crystals of each functionalization exhibit a rod-like geometry. The diameter and length of each rod highlighted in Figure 2(a)-2(c) are measured from the topographic images and summarized in Table I below. The diameters determined from the height of AFM images of CNCs, DS-CNCs and AQ-CNCs fall within the range of 2.5-3.5 nm. Since individual CNCs exhibited very similar diameters and length upon treatments of desulfation followed by anthraquinone functionalization, the structural integrity of the individual fibers remains.

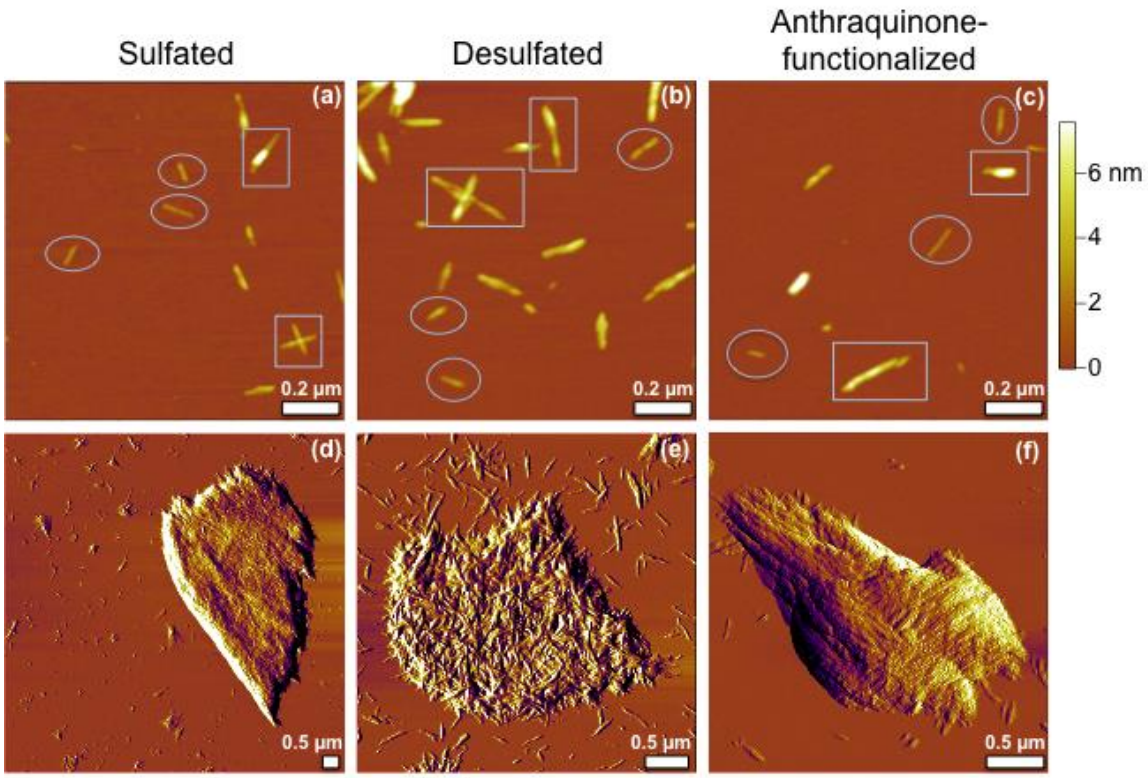

Figure 2: AFM topographic images (1.2 µm x 1.2 µm) of (a) CNCs, (b) DS-CNCs, and (c) AQ-CNCs. All images were acquired using tapping mode in ambient. Scale bars = 0.2 µm. AFM amplitude images of aggregates are shown for (d) CNCs, (e) DS-CNCs and (f) AQ-CNCs samples.

Table 1: Dimensions of individual CNCs measured from Figure 2 images (a)-(c).

Samples	Diameter (nm) / Length (nm)		
CNC	2.8/ 115.6	2.5/ 80.6	2.6/ 72.9
DS-CNC	3.0/ 89.7	3.5/ 73.4	3.1/ 118.6
AQ-CNC	3.0/ 99.1	2.8/ 61.6	2.5/ 132.1

The AFM topographic images also reveal the presence of bundles of rods for each sample. Examples of these bundles are indicated by rectangular enclosures. In the two CNC bundles shown in Figure 2(a), one is a cross of 131.5 and 110.5 nm rods, and the other is a short rod (77.4 nm) completely atop of a rod (173.8 nm), resulting in the bright contrast seen in the AFM topograph. In the two DS-CNC bundles shown in Figure 2(b), the topmost bundle is composed of three rods: the bottom long rod (225.7 nm) supporting two short rods (51.7 and 70.5 nm, respectively), completely atop, appearing as two brighter contrasts. The top left bundle is composed of three rods: two rods (219.1 and 169.1 nm) overlapped side-by-side, with the 3rd rod (167.6 nm) stacking perpendicularly atop, leading to a cross shape. In the two AQ-CNC bundles, the bundle in the upper right of image 2(c) consists a 68.1 nm rod stacked atop of a 117.4 nm rod completely. The bundle in the lower left of Figure 2(c) consists of three rods: a 91.9 nm long rod attached to the surface, with a small 56.7 nm rod aligned next to the right end, and the third 134.5 nm rod stacked at an angle on top of the end of the rod beneath it. In contrast to the CNCs and DS-CNCs which exhibit branched bundles, the bundles in the AQ-CNC samples mostly consist of aligned rods, which are advantageous for subsequent production of composite materials.

For all three types of CNCs, large aggregates were occasionally seen. In Figure 2(d), the AFM amplitude image clearly reveals the individual CNC rods within the “flake-shaped” aggregate (maximum lateral dimension of 6.6 μm wide), which are aligned in parallel with respect to each other. Simultaneously, the topographic image (not shown) reveals the height of the aggregate as 226.7 nm, which is equivalent to 86 layers of individual crystals. In Figure 2(e), the AFM amplitude image shows the individual rods within the “haystack” aggregate of the DS-CNCs (with a maximum lateral dimension of 3.1 μm), adopting random orientations. The AFM topographic image (not shown) reveals the height of the aggregate is 67.8 nm, which is equivalent to 21 layers of individual crystals. In Figure 2(f), the AFM amplitude image reveals the “interwoven” arrangement of the individual AQ-CNC rods within the “tadpole-shaped” aggregate (maximum lateral dimension of 2.8 μm). The AFM topographic image (not shown) shows the aggregate’s height as 206.7 nm, which is equivalent to 75 layers of individual crystals. Even though the aggregates are a minority population, from this AFM investigation we recommend caution to prevent them when processing AQ-CNCs, as the AQ-CNC aggregates would be more difficult to disperse due to the interwoven packing.

3.2 Effects of reaction conditions on grafting efficiency

In order to optimize the grafting efficiency of AQ on CNCs, the conditions for the two mains steps of the esterification reaction were varied. The first step of the esterification reaction is the formation of an AQC intermediate with the CDI, which was controlled by varying the molar ratio of CDI to AQC. For the second step of the reaction, the reaction time and ratio of anhydroglucose unit (AGU) to AQC and CDI were varied. To quantify the effects of these changes, intensity ratios of the ester bond peak (1725 cm^{-1}) to the C-H bond peak (2898 cm^{-1}) were assumed to be equivalent to the relative abundance of covalently linked AQ groups on the CNC surface. The ester peak is attributed the covalent linkage of AQ to CNC and the C-H bond peak is unaffected by the reaction and thus serves as an internal standard [20]. In addition, UV-vis measurements of the anthraquinone groups on AQ-CNC samples were conducted and yields of the grafting reaction of AQC on CNCs were calculated based on a calibration curve.

Figure 3(a) shows the FTIR band ratios of 1725 cm^{-1}/2898 cm^{-1} and grafting yields under varied molar ratios of AQC/CDI. With the increase of the CDI amount in the reaction system, the peak ratios of 1725 cm^{-1}/2898 cm^{-1} in FTIR spectra of produced AQ-CNC samples increased

correspondingly. CDI reacts with the carboxylic acid group on AQC and is highly sensitive to moisture. By increasing the amount of CDI relative to AQC, the losses due to moisture during the reaction can be compensated for. Measurements of UV-vis spectrometry of AQ-CNC samples also show an increase of the grafting yields of AQC on CNCs (Figure 3(a)) with increasing CDI, verifying its importance to the incorporation of AQC onto the CNC surfaces.

To further optimize reaction yield, the AGU/AQC/CDI molar ratio to the grafting esterification reaction was investigated. However, when the AGU/AQC ratio is changed, the amount of CDI also needs to be changed so that the AQC/CDI relationship is kept consistent to enable maximum formation of the AQC intermediate. To this end, the AQC/CDI ratio was kept around 1: 2- 1: 2.5 when the AGU/AQC ratio was changed from 1: 1 to 1: 4. Such a small variation in the ratio of AQC/CDI should have little impact on the yield changes seen in the varied ratios of AGU/AQC. FTIR results indicated that the esterification reaction was improved as the AGU/AQC ratio was increased in the system, as evidenced by the increased esterification ratios and grafting yields shown by peak ratios of 1725 cm^{-1}/2898 cm^{-1} (Figure 3(b)), which was verified by UV-vis absorbance of AQ-CNCs. Higher concentrations of AQC means that it is more readily available for incorporation, and helps to drive the reaction forward, resulting in an increase in reaction yields. Thus, both ratios of AQC/CDI and AQC/AGU are important in optimizing the esterification reaction and driving the reaction forward to increase product formation.

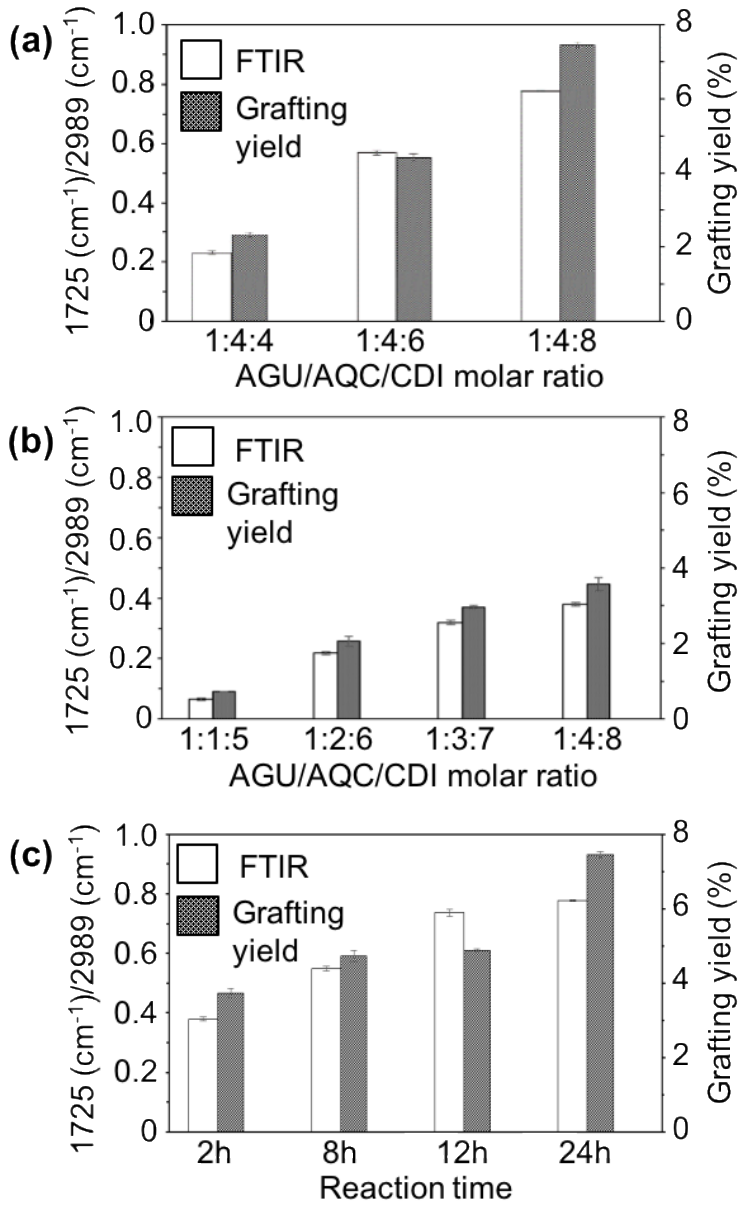

Figure 3. Impacts of reaction conditions on ester formation, shown in ratios of 1725 cm^{-1}/2989 cm^{-1} and grafting yields. (a) Impact of ratios of AQC/CDI (AGU/AQC unchanged), (b) impact of ratios of AGU/AQC/CDI, (c) impact of reaction time.

The esterification products (AQ-CNCs) also increase as the reaction time increases, as shown in Figure 3(c). The molar ratio of AGU/AQC/CDI was kept constant at 1: 4: 8, yet the ratio of 1725 cm^{-1}/2898 cm^{-1} increased from 0.380 within 2 hours to 0.777 at 24 hours, doubling the yield. The grafting ratios characterized by the UV-vis spectroscopy verifies the same trend of increasing AQ incorporation as the reaction time increased from 2 to 24 hours. Both measurements of AQ incorporation support the conclusion that increased exposure of AGU to AQC leads to increased incorporation of AQ on the CNCs.

3.3 Photo-activities of AQ-CNCs

Anthraquinone derivatives possess photo-activities, and when AQ was chemically incorporated onto cellulosic materials, the desired light-induced antibacterial functionality was achieved. The overall photo-initiated functional process is caused by excitation of AQ to its excited singlet status, which quickly undergoes intersystem crossing to its triplet status. The triplet AQ abstracts a hydrogen atom from a weak C-H bond in cellulose to become AQH radical, which reacts with triplet oxygen to result in reactive oxygen species such as hydroxyl radicals and hydrogen peroxide [11]. To verify that this process remained intact and that the AQ-CNCs possess the light

induced functionality, the amount of reactive oxygen species (ROS) produced needs to be evaluated. One of the ROS produced, hydroxyl radicals, can be detected and quantified using an indirect spectrophotometrical method involving a hydroxyl radical scavenger, p-nitrosodimethylaniline (p-NDA) [7]. The bleaching rates of p-NDA for the varied synthesis conditions of AQ-CNCs were determined by monitoring the absorption of each solution at a wavelength of 440 nm after exposure to UVA (365 nm) light. The results are shown in Figure 4(a) and Figure 4(b).

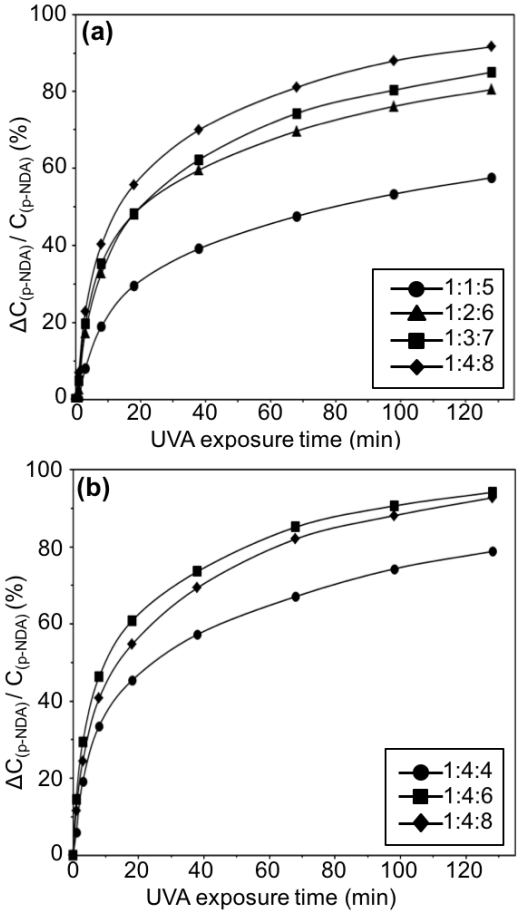

Figure 4. Photo-bleaching rates of p-NDA under UVA by AQ-CNCs made from (a) varied AQC/AGU molar ratios at a reaction time of 2 hours and (b) varied AQC/CDI molar ratios at a reaction time of 24 hours.

According to the results shown in Figure 4(a), the photo-bleaching rate accelerated as the ratio of AGU/AQC/CDI increases, consistent with the photo-activity of AQ structure and increased AQ loading on AQ-CNCs. When the UVA irradiation time increased, the amount of hydroxyl radicals cumulatively increased as well. However, in Figure 4(b), after reaction of 24 hours the AQ-CNC sample made with a molar ratio of AGU/AQC/CDI at 1: 4: 8 with a measured grafting ratio of 7.454 wt.% demonstrated a similar but slightly lower photo-bleaching power than that of the sample made in a molar ratio of 1:4:6 with a grafting ratio of 4.428 wt.%. This phenomenon reveals a potential saturation of the photo-activity on the AQ-CNCs over time. Too high of a concentration of AQ groups on AQ-CNCs may interfere with the formation of triplet structure of AQ and inhibit the abstraction of hydrogen atoms from the connected cellulose rings, since all AQ structures are chemically grafted on close vicinity of the surfaces of the CNCs.

To further verify the photoactivity of AQ-CNCs, the hydrogen peroxide produced in aqueous condition was measured by using an iodometric method under UVA light irradiation. The absorbance of the mixture was measured spectrophotometrically at 351 nm, and the amount of H_2O_2 in the DI water was calculated according to a standard calibration curve. The results are shown in Figures 5(a) and 5(b).

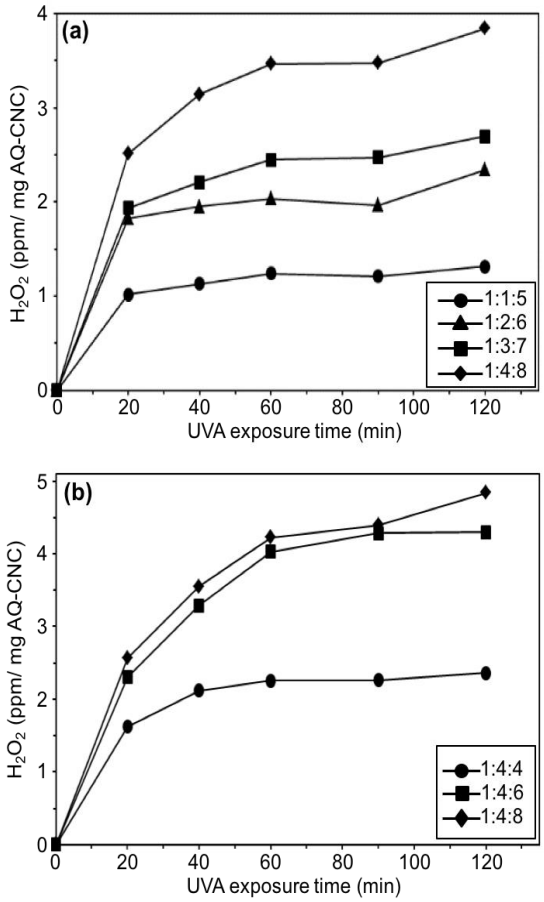

Figure 5. Amounts of hydrogen peroxide produced under UVA (a) by AQ-CNCs made from varied AGU/AQC molar ratios at reaction time of 2 hours, and (b) by AQ-CNCs made from varied AQC/CDI molar ratios at reaction time of 24 hours.

Based on Figure 5(a), the amounts of hydrogen peroxide formed increased as the UVA exposure time was prolonged. The AQ-CNC samples containing more AQC units generated more hydrogen peroxide in the solutions, consistent with the p-NDA bleaching results. However, in Figure 5(b), the AQ-CNC sample with a grafting rate of 4.428 wt.% exhibited similar amounts of hydrogen peroxide in comparison to that of the one with the highest grafting ratio one of 7.454 wt.% at 90 minutes exposure time. This outcome matches the previous abnormal results of the measured hydroxyl radicals, indicating the saturation of photo-activities at high concentration of AQ loading at higher exposure times. Further investigation of the photo activity of AQ-CNCs revealed an interesting phenomenon from these materials, i.e. the continued generation of hydroxyl radicals even after the UVA irradiation was terminated. The three AQ-CNC samples containing 2.333 wt.% (1:4:4 molar ratio), 4.428 wt.%, 7.454 wt.% of AQ moieties from Figure 5(b) were tested, and all exhibited persistent photo-bleaching ability against p-NDA after UVA exposure was terminated (Figure 6(b)), indicating the generation of hydroxyl radicals without direct light irradiation. The more AQ units grafted onto CNCs, the better photo-bleaching efficiency of the samples was, indicating that sustained ROS generation efficacy is dependent on AQ loading on CNC. This unexpected phenomenon could be caused by an unusual property possessed by some anthraquinone derivative structures, the so called light-absorbing transient behavior [23,24].

A proposed mechanism for this light absorbing transient behavior is shown below in Figure 6(a). The light-absorbing transient (LAT)s are quasi-stable intermediates resulting from relatively

stable radical terminations[23-24]. The excited triplet AQ structures on AQ-CNCs could abstract a hydrogen atom from a hydrogen donor site on CNCs to form AQH radical intermediates (Figure 6(a)), which are the light-absorbing transient structures similar to that of benzophenone radicals reported in literatures [23,24]. Due to the delocalization of electrons in the of AQH radicals (as explained by the existence of resonance structures), these LAT structures are more stable. The light-absorbing transient structures can react with oxygen and other species, generating reactive oxygen species (ROS) such as hydroxyl radicals, perhydroxyl radicals, and hydrogen peroxide [7,11]. The oxygen consumption plays an important role in the photoreaction in the presence of hydrogen donor. It has been reported that the decay of the light-absorbing transient photoproducts is accelerated on exposure to oxygen [25,26].

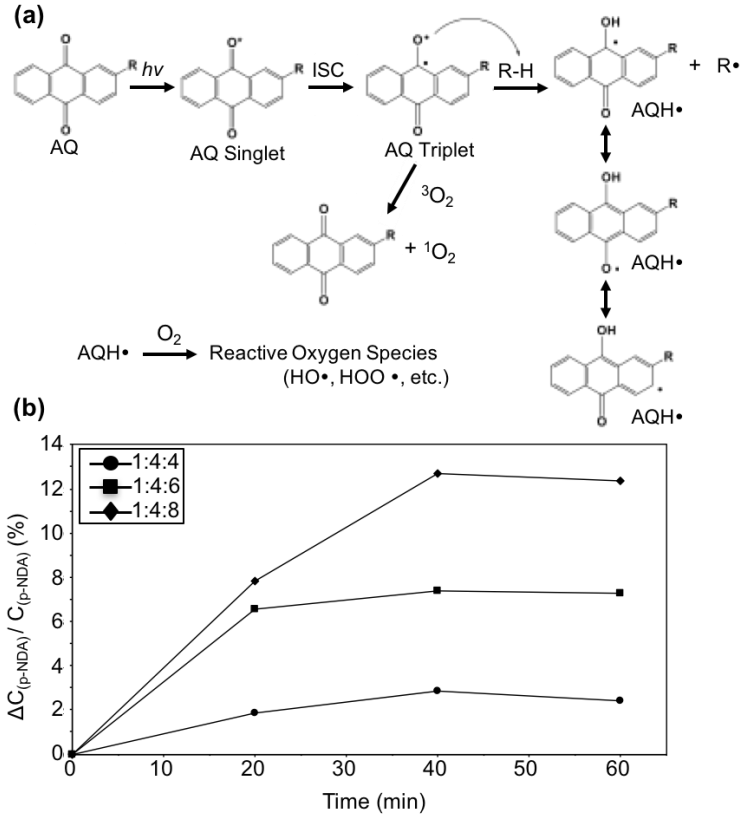

Figure 6. (a) Scheme of the photo-reaction of AQ derivatives with R-H (cellulose) and formation of ROS; (b) Generation of hydroxyl radicals in darkness by AQ-CNCs from varied AQC/CDI molar ratios.

3.4 Stability of light active AQ-CNCs

Based on the photo-bleaching reactions of p-NDA demonstrated by AQ-CNC samples under or without UVA exposure, formation of excited AQ and radical AQH (and conjugate) structures in ambient conditions is key. CNCs serve as effective hydrogen donors (R-H) directly connected to AQ, enabling easier hydrogen abstraction and thus formation of AQH. The ease of AQH formation enabled by the CNCs proximity may help to compensate for radical AQH quenching caused by oxygen exposure, leading to prolonged lifetimes of the radical AQH and the persistent generation of ROS under darkness. Interestingly, the AQH transient structures were quite stable and could store the light-induced energy for several days, as most of the tests on the AQ-CNCs under dark were conducted several days after being sealed in darkness.

4. Conclusions

We have successfully demonstrated a direct esterification reaction between cellulose nanocrystals (CNCs) and anthraquinone carboxylic acid (AQC) for the first time. This covalent binding was verified by FTIR and UV-vis spectroscopy. The morphology and photoactivity were characterized following the covalent reactions. AFM revealed that the CNCs retain structural integrity, an advantage for subsequent making of composite materials. AQ-CNCs are highly

photoactive under daylight or UVA, generating both hydroxyl and hydrogen peroxide radicals. The quantity of radicals increases with increasing UVA exposure time or concentration of AQC on CNCs up to a point. More interestingly, AQ-CNCs formed light-absorbing transient structures that store the light-excited structures and provide effective bleaching of p-NDA under darkness. The AQ-CNC based materials offer a promising candidate towards developing green, photoactive hybrid materials with self-disinfecting properties.

Author Contributions: Conceptualization, Yiwen Zhu[1] and Audrey Sulkanen[2]; methodology, Yiwen Zhu[1] and Audrey Sulkanen[2]; validation, Yiwen Zhu[1] and Audrey Sulkanen[2]; formal analysis, Yiwen Zhu[1], Gang Sun[1]*, Gang-Yu Liu[2] and Audrey Sulkanen[2]; investigation, Yiwen Zhu[1] and Audrey Sulkanen[2]; resources, Gang Sun[1]* and Gang-Yu Liu[2]; writing—original draft preparation, Gang Sun[1]*; writing—review and editing, Yiwen Zhu[1], Gang Sun[1]*, Gang-Yu Liu[2] and Audrey Sulkanen[2]; visualization, Yiwen Zhu[1] and Audrey Sulkanen[2]; supervision, Gang Sun[1]* and Gang-Yu Liu[2]; project administration, Yiwen Zhu[1] and Audrey Sulkanen[2]; funding acquisition, Yiwen Zhu[1] and Audrey Sulkanen[2]. All authors have read and agreed to the published version of the manuscript.

Funding: This research was funded in part by National Science Foundation (CHE-1808829), the Henry A. Jastro Graduate Student Research Scholarship of College of Agricultural and Environmental Sciences and the Summer Graduate Student Researcher (GSR) Award of University of California, Davis.

Conflicts of Interest: The authors declare no conflict of interest. The funders had no role in the design of the study; in the collection, analyses, or interpretation of data; in the writing of the manuscript, or in the decision to publish the results.

References

1. Foorginezhad, S.; Zerafat, M.M. Fabrication of stable fluorine-free superhydrophobic fabrics for anti-adhesion and self-cleaning properties. *Applied Surface Science* **2019**, *464*, 458-471, doi:https://doi.org/10.1016/j.apsusc.2018.09.058.
2. Doganli, G.; Yuzer, B.; Aydin, I.; Gultekin, T.; Con, A.H.; Selcuk, H.; Palamutcu, S. Functionalization of cotton fabric with nanosized TiO2 coating for self-cleaning and antibacterial property enhancement. *Journal of Coatings Technology and Research* **2016**, *13*, 257-265, doi:10.1007/s11998-015-9743-7.
3. Ma, Y.; Zhang, Z.; Nitin, N.; Sun, G. Integration of photo-induced biocidal and hydrophilic antifouling functions on nanofibrous membranes with demonstrated reduction of biofilm formation. *Journal of Colloid and Interface Science* **2020**, *578*, 779-787, doi:https://doi.org/10.1016/j.jcis.2020.06.037.
4. Zhuo, J. Photochemical Study of Anthraquinone Derivatives and Their Applications (Doctoral dissertation. University of California, Davis, 2016.
5. Gao, A.; Zhang, H.; Sun, G.; Xie, K.; Hou, A. Light-induced antibacterial and UV-protective properties of polyamide 56 biomaterial modified with anthraquinone and benzophenone derivatives. *Materials & Design* **2017**, *130*, doi:10.1016/j.matdes.2017.05.071.
6. Zhuo, J. Photoactive chemicals for antimicrobial textiles. In *Antimicrobial Textiles*, Sun, G., Ed. Woodhead Publishing: 2016; pp. 197-223.
7. Liu, N.; Sun, G. Production of Reactive Oxygen Species by Photoactive Anthraquinone Compounds and Their Applications in Wastewater Treatment. *Industrial & Engineering Chemistry Research* **2011**, *50*, 5326-5333, doi:10.1021/ie101423v.
8. Zhuo, J.; Sun, G. Antimicrobial functions on cellulose materials introduced by

anthraquinone vat dyes. *ACS Appl Mater Interfaces* **2013**, *5*, 10830-10835, doi:10.1021/am403029w.

9. Gorner, H. Photoinduced oxygen uptake for 9,10-anthraquinone in air-saturated aqueous acetonitrile in the presence of formate, alcohols, ascorbic acid or amines. *Photochem Photobiol Sci* **2006**, *5*, 1052-1058, doi:10.1039/b606968a.
10. Zhang, Z.; Si, Y.; Sun, G. Photoactivities of Vitamin K Derivatives and Potential Applications as Daylight-Activated Antimicrobial Agents. *ACS Sustainable Chemistry & Engineering* **2019**, *7*, 18493-18504, doi:10.1021/acssuschemeng.9b04449.
11. Liu, N.; Sun, G.; Zhu, J. Photo-induced self-cleaning functions on 2-anthraquinone carboxylic acid treated cotton fabrics. *Journal of Materials Chemistry* **2011**, *21*, 15383-15390, doi:10.1039/c1jm12805a.
12. Rajinipriya, M.; Nagalakshmaiah, M.; Robert, M.; Elkoun, S. Importance of Agricultural and Industrial Waste in the Field of Nanocellulose and Recent Industrial Developments of Wood Based Nanocellulose: A Review. *ACS Sustainable Chemistry & Engineering* **2018**, *6*, 2807-2828, doi:10.1021/acssuschemeng.7b03437.
13. Yildirim, N.; Shaler, S. A Study on Thermal and Nanomechanical Performance of Cellulose Nanomaterials (CNs). *Materials* **2017**, *10*, doi:10.3390/ma10070718.
14. Jonoobi, M.; Oladi, R.; Davoudpour, Y.; Oksman, K.; Dufresne, A.; Hamzeh, Y.; Davoodi, R. Different preparation methods and properties of nanostructured cellulose from various natural resources and residues: a review. *Cellulose* **2015**, *22*, 935-969, doi:10.1007/s10570-015-0551-0.
15. Natterodt, J.; Fink, A.; Weder, C.; Zoppe, J. Cellulose Nanocrystals: Surface Modification, Applications and Opportunities at Interfaces. *CHIMIA International Journal for Chemistry* **2017**, *71*, 376-383, doi:10.2533/chimia.2017.376.
16. Börjesson, M.; Sahlin, K.; Bernin, D.; Westman, G. Increased thermal stability of nanocellulose composites by functionalization of the sulfate groups on cellulose nanocrystals with azetidinium ions. *Journal of Applied Polymer Science* **2018**, *135*, 45963, doi:10.1002/app.45963.
17. Hasani, M.; Cranston, E.D.; Westman, G.; Gray, D.G. Cationic surface functionalization of cellulose nanocrystals. *Soft Matter* **2008**, *4*, 2238-2244, doi:10.1039/b806789a.
18. Jiang, F.; Esker, A.R.; Roman, M. Acid-catalyzed and solvolytic desulfation of H2SO4-hydrolyzed cellulose nanocrystals. *Langmuir* **2010**, *26*, 17919-17925, doi:10.1021/la1028405.
19. Braun, B.; Dorgan, J.R.; Chandler, J.P. Cellulosic nanowhiskers. Theory and application of light scattering from polydisperse spheroids in the Rayleigh-Gans-Debye regime. *Biomacromolecules* **2008**, *9*, 1255-1263, doi:10.1021/bm7013137.
20. Hou, A.; Sun, G. Multifunctional finishing of cotton fabrics with 3,3',4,4'-benzophenone tetracarboxylic dianhydride: reaction mechanism. *Carbohydr Polym* **2013**, *95*, 768-772, doi:10.1016/j.carbpol.2013.02.027.
21. Peralta, M.D.R.; Karsai, A.; Ngo, A.; Sierra, C.; Fong, K.T.; Hayre, N.R.; Mirzaee, N.; Ravikumar, K.M.; Kluber, A.J.; Chen, X., et al. Engineering Amyloid Fibrils from

β-Solenoid Proteins for Biomaterials Applications. *ACS Nano* **2015**, *9*, 449-463, doi:10.1021/nn5056089.

22. Gu, J.; Catchmark, J.M.; Kaiser, E.Q.; Archibald, D.D. Quantification of cellulose nanowhiskers sulfate esterification levels. *Carbohydr Polym* **2013**, *92*, 1809-1816, doi:10.1016/j.carbpol.2012.10.078.
23. Görner, H. Involvement of light absorbing transients upon photoreduction of 4-benzoylpyridine and 4,4′-dipyridylketone via donor and acceptor radicals. *Chemical Physics* **2008**, *344*, 264-272, doi:https://doi.org/10.1016/j.chemphys.2008.01.011.
24. Si, Y.; Zhang, Z.; Wu, W.; Fu, Q.; Huang, K.; Nitin, N.; Ding, B.; Sun, G. Daylight-driven rechargeable antibacterial and antiviral nanofibrous membranes for bioprotective applications. *Sci Adv* **2018**, *4*, eaar5931, doi:10.1126/sciadv.aar5931.
25. Pitts, J.N.; Letsinger, R.L.; Taylor, R.P.; Patterson, J.M.; Recktenwald, G.; Martin, R.B. Photochemical Reactions of Benzophenone in Alcohols1. *Journal of the American Chemical Society* **1959**, *81*, 1068-1077, doi:10.1021/ja01514a014.
26. Chilton, J.; Giering, L.; Steel, C. The effect of transient photoproducts in benzophenone-hydrogen donor systems. *Journal of the American Chemical Society* **1976**, *98*, 1865-1870, doi:10.1021/ja00423a036.